applied sciences

MDPI

Article

A Novel Technique for Designing High Power Semiconductor Optical Amplifier (SOA)-Based Tunable Fiber Compound-Ring Lasers Using Low Power Optical Components

Muhammad A. Ummy [1,*], Simeon Bikorimana [2] and Roger Dorsinville [2]

1 New York City College of Technology, City University of New York, New York, NY 11201, USA
2 The City College of New York, City University of New York, New York, NY 10031, USA; sbikori00@citymail.cuny.edu (S.B.); rdorsinville@ccny.cuny.edu (R.D.)
* Correspondence: maummy@citytech.cuny.edu; Tel.: +1-718-260-5300

Academic Editor: Malte C. Kaluza
Received: 1 April 2017; Accepted: 3 May 2017; Published: 5 May 2017

Abstract: A simple, stable and inexpensive dual-output port widely tunable semiconductor optical amplifier (SOA)-based fiber compound-ring laser structure is demonstrated. This unique nested ring cavity enables high optical power to split into different branches where amplification and wavelength selection are achieved by using low-power SOAs and a tunable filter. Furthermore, two Sagnac loop mirrors, which are spliced at the two ends of the compound-ring cavity not only serve as variable reflectors but also channel the optical energy back to the same port without using any high optical power combiner. We propose and discuss how the demonstrated fiber compound-ring laser structure can be extended in order to achieve a high power fiber laser source by using low power optical components, such as $N \times N$ couplers and ($N > 1$) number of SOAs. A coherent beam-combining efficiency of over 98% for two parallel nested fiber ring resonators is achieved over the C-band tuning range of 30 nm. Optical signal-to-noise ratio (OSNR) of +45 dB, and optical power fluctuation of less than ± 0.02 dB are measured over three hours at room temperature.

Keywords: semiconductor optical amplifier; beam combining; power scalability; Sagnac interferometer; laser tuning; ring laser

1. Introduction

Single-mode fiber resonators of different architectures such as linear [1], Fox-Smith [2], ring [3–5], and compound fiber ring [6–9] cavities have been theoretically and experimentally explored in designing and building various kinds of fiber laser sources with single-longitudinal mode operation for low and high optical power applications such as optical communication systems, and for scientific, medical, material processing and military purposes [10]. Adjustable, scalable output optical power and wavelength tunability properties of a fiber laser source are of a great interest in the aforementioned applications that require high optical power. Complex and expensive in-line variable optical attenuators (VOAs) with adjustable insertion losses are usually used to control the output optical power level of laser sources. Mechanical, micro-electromechanical [11–13], acousto-optic [14], and electro-wetting [15] methods as well as optical fiber tapers [16] and hybrid microstructure fiber-based techniques [17] are widely used to adjust the insertion losses of the in-line fiber-based VOAs. However, all-fiber-based low power variable reflectors or mirrors such as Sagnac loop mirrors (SLMs) can also be used to control the amount of optical power from low and high power fiber laser sources. All-single-mode fiber-based Sagnac loop mirrors have been widely used in temperature [18], strain [19], and pressure [20] high sensitivity sensors as well as in wavelength optical switches [21]. Moreover, SLMs with adjustable reflectivity have been used to form Fabry–Perot linear resonators [22–25] where the amount of the output optical power from the resonators depends on the reflectivity of the SLMs [26,27]. In this work, two SLMs were used to control the amount of optical power delivered from two output ports of the proposed fiber compound-ring laser. In addition, two inexpensive low power semiconductor optical amplifiers (SOAs) were placed in two parallel nested ring cavities to demonstrate the possibility of achieving a highly power scalable, adjustable and switchable fiber laser structure based on multiple nested compound-ring cavities formed by N $\times$ N fiber couplers with two SLM-output couplers.

Different methods have been utilized to scale up optical power of laser sources where beam combining has shown to be a promising alternative technique of achieving high power by scaling up multiple combined laser elements. High power laser sources with high beam quality have been demonstrated by using complex coherent and spectral beam-combining techniques in external cavities [28–35]. In addition, incoherent beam-combining method [36,37] has been used to scale up the optical power by combining individual laser elements as well. Michelson and Mach-Zehnder resonators were mostly used in coherent beam combining in order to achieve high combining efficiency and almost diffraction-limited beam quality [38–40]. More importantly, ring resonators have proven to be efficient and stable [41] for a passive coherent beam-combining method. In order to achieve high power laser sources with high combining efficiency, all the aforementioned methods require sophisticated high power external optical components such as micro-lenses, isolators, circulators, photonic crystal fibers and master oscillator pre-amplifiers that are usually complex and very expensive. In addition, rare-earth, ytterbium doped fiber amplifiers (YDFAs) [41] or erbium doped fiber amplifiers (EDFAs) [42] that are usually used as gain media for beam combining to achieve high power laser systems with different types of cavity structures such as Y-shaped linear cavities also need to be pumped with other types of laser sources, which makes them very inefficient. However, by using nested compound-ring cavities where circulating beams are equally split in N-number of low power beams that can be amplified by N-number of low power SOAs, one can achieve a highly efficient high power laser system that does not require the extra pump lasers, master oscillator pre-amplifiers or other expensive external high power optical components.

Semiconductor optical amplifiers (SOAs) [43], stimulated Raman scattering (SRS) amplifiers [44,45] and stimulated Brillouin scattering (SBS) amplifiers [46,47] have also been used as gain media in different fiber laser systems. However, the SOAs are more advantageous than their above-mentioned counterparts because they are compact, light, less expensive, efficient, and available for different operational regions from a wide range of wavelength spectra. In particular, SOAs have the capability to be integrated with other InP (Indium phosphide)-based optical components, which makes it more attractive to implement very high compact optical systems. Extensive theoretical studies and analysis of SOA-based optical systems have shown that they can be used for several applications, such as compact SOA-based laser rangefinders [48], optical pulse delay discriminators [49,50], and optical and logic gates [51] for high-speed optical communications by exploiting four-wave mixing [52,53]. In addition, note that when the SOAs are used in a bidirectional fiber ring resonator structure, such as the proposed one, they do not require extra optical components, for instance, optical isolators and optical circulators; as a result, they are easy to integrate with other optical components for compact fiber laser systems. Semiconductor optical amplifiers have also been used along with erbium doped fiber amplifiers in order to suppress optical power fluctuation in a pulsed lightwave frequency sweeper where the suppression of power fluctuation is attributed to the gain saturation and fast response of the SOA [54,55].

In this work, we demonstrate a novel technique for a coherent beam-combining method based on the passive phase-locking mechanism [56–58] of two C-band low power SOAs-based all-single-mode fiber compound-ring resonators by exploiting beam combining (i.e., interference) at 3-dB fiber couplers that connect two parallel merged ring cavities. This is unlike previous work [59] where non-adjustable multimode fiber laser output formed by a high power and expensive power combiner with a multimode output fiber (i.e., low brightness) was replaced by two low power Sagnac loop mirrors to create a dual-output port all-single-mode fiber laser structure with switchable and adjustable output power. In addition, the single-mode performance is maintained in order to improve the brightness at the proposed fiber compound-ring laser output port. The output power of the proposed combined fiber compound-ring resonators with two low power SOAs was almost twice as large as the output power obtained from a single SOA-based fiber ring or the Fabry–Perot linear resonator [25]. More than 98% beam combining efficiency of two parallel nested fiber ring resonators is demonstrated over the C-band tuning range of 30 nm. Optical signal-to-noise ratio (OSNR) +45 dB, and optical power fluctuation of less than $\pm$0.02 dB are measured over three hours at room temperature.

The main characteristics of the proposed fiber compound-ring laser, power tunability, and switchable output port can find applications in long-distance remote sensing [60]. Moreover, its wide range wavelength tunability can benefit several applications in fiber sensors [61–65] and wavelength division multiplexer (WDM) optical communications [66] as well as biomedical imaging systems [67] working in the third near infrared biological window [68].

Finally, we discuss on how to achieve a highly power-scalable fiber compound-ring laser system using low power and inexpensive optical components such as tunable filter and low power SOAs.

2. Experimental Setup

Figure 1 illustrates the experimental schematic diagram of the C-band SOA-based tunable fiber laser with two nested ring cavities (i.e., compound-ring resonator) and two broadband Sagnac loop mirrors that serve as either dual-output ports or a single output port according to the reflectivity settings of each of the Sagnac interferometers (i.e., SLMs). Each ring cavity consists of two branches, I-II and I-III, for the inner and the outer ring cavity, respectively. Both ring cavities share a common branch, I, which contains an SOA_1, (Kamelian, OPA-20-N-C-SU), a tunable optical filter (TF-11-11-1520/1570), and a polarization controller, PC_1. Branch II contains an SOA_2 (Thorlabs, S1013S), and a polarization controller, PC_2. Branch III contains only a polarization controller, PC_3. Note that the branch has no SOA due to the limited number of SOAs available during the time of our experiment. All the three branches, I, II and III, are connected by two 3-dB fiber couplers, C_1 and C_2. Each 3-dB fiber coupler, C_1 and $C_{2,}$ is also connected to a Sagnac loop mirror, SLM_1 and SLM_2, respectively, as shown in Figure 1. These Sagnac loop mirrors, with a polarization controller placed in each loop, act as variable reflectors. By adjusting the polarization controller (i.e., PC_4 or PC_5), one can change the reflectivity of the loop mirrors and thereby can switch from single to dual-output port configurations [26,27]. The low power tunable optical filter (TF), which is placed in the common branch I, is used for selecting and tuning the operating wavelength of the proposed fiber laser. It operates between 1520 and 1570 nm wavelength. There are three PCs (PC_1, PC_2 and PC_3) in the compound-ring resonator.

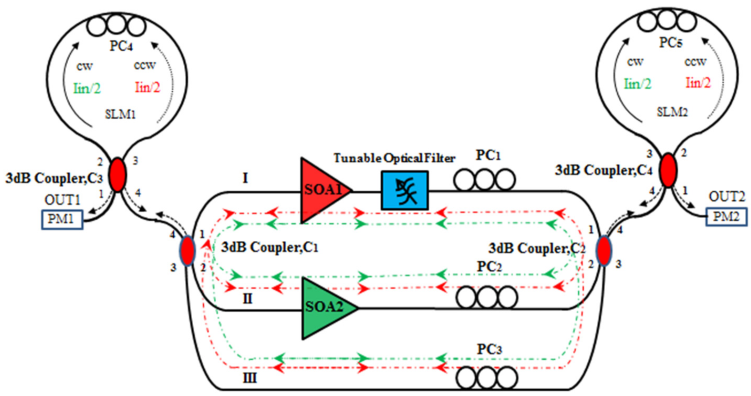

Figure 1. Experimental setup of the dual Sagnac loop mirror semiconductor optical amplifier (SOA)-based tunable fiber compound-ring laser. PC: polarization controller; cw: clockwise; ccw: counter-clockwise, SLM: Sagnac loop mirrors; PM: power meter.

3. Principal of Operation

When the pump level (i.e., bias current threshold level) of either SOA is more than the total fiber compound-ring cavity losses, amplified spontaneous emission (ASE) emitted from SOAs either propagates in the forward and backward directions. For instance, when a bias current I_B of around 75 mA) is injected into the SOA_1 (branch I), the ASE (Amplified Spontaneous Emission) emitted by the SOA_1 (branch I) circulates in clockwise (cw) direction by propagating through a tunable optical filter, which selects a passband of certain wavelengths. The selected wavelengths reach a 3-dB fiber coupler C_2 after propagating through a polarization controller, PC_1. Then, the selected light beam that arrives at port 1 of the 3-dB fiber coupler C_2, is equally split into two branches, II and III at port 2 and port 3, respectively. The light beam that circulates into branch II propagates through a polarization controller, PC_2, before it is amplified by SOA_2 when its bias current level, I_B, is around 180 mA. Then, the amplified light beam arrives at port 2 of the 3-dB fiber coupler C_1 where it is equally divided between port 1 and port 4. Similarly, light beam from Branch III reaches port 3 after passing through a polarization controller, PC_3. Half of the light beam coupled into port 1 of the 3-dB fiber coupler C_1 is further amplified by SOA_1. Thus, a round-trip is completed in the fiber compound-ring structure and allows lasing to occur. Furthermore, the remaining 50% of the light beam is coupled into the output port 4 of the 3-dB fiber coupler C_1 is injected into the input port 4 (i.e., I_{in}) of the Sagnac loop mirror, SLM_1. The polarization controller, PC_4, controls the reflectivity of the SLM_1 and it is achieved by adjusting the state of polarization of the light beams propagating through the Sagnac loop mirror. For a single output port configuration, the polarization controller PC_4 of SLM_1 is adjusted for minimum power at the output port 1 (OUT1). The counterclockwise and clockwise light beams interfere destructively at the output port 1 while they interfere constructively at port 4 of the 3-dB fiber coupler, C_3, and thus it channels all the power back to the compound-ring cavity.

As there is no optical isolator placed in any of the three branches of the fiber compound-ring resonator, the two counter-propagating light beams circulate in the nested ring cavities as shown in Figure 1. The counter-clockwise (ccw) propagating beam from the SOA_1 reaches the port 1 of the 3-dB coupler C_1, splits into two equal light beams (i.e., 50%) and is transmitted into the ports 2 and 3. The light beam that propagates into branch II undergoes amplification by $SOA_{2.}$ The amplified light beam that takes the path of branch II passes through a polarization controller PC_2 before it reaches port 2 of the 3-dB fiber coupler C_2, while the light beam that propagates through the branch III passes through the polarization controller PC_3 before it reaches port 3 of the 3-dB fiber coupler C_2. Half of the light beam at the 3-dB fiber coupler C_2 is coupled into port 1 where it propagates back into branch I to complete one round trip, while the other half of the beam is channeled into SLM_2. Similarly, the light beam that is fed into the SLM_2 exits at the output port 1 of the 3-dB fiber coupler C_4 (OUT2). The output power can be controlled by the polarization controller, PC5. An optical spectrum analyzer (OSA), variable optical attenuator (VOA) and optical power meter (PM) were used to characterize the proposed fiber compound-ring laser. Note that the path lengths of both loops are the same since all branches have identical length and all fiber connections are done by using FC/APC (Fiber channel/Angled polished Connector) connectors.

4. Characterization of the Fiber Compound-Ring Lasers

4.1. Gain Medium

The amplified spontaneous emission (ASE) of SOA_1, and SOA_2 were characterized by using an optical spectrum analyzer (OSA) where both SOAs were set at the same bias current (I_B) of 200 mA. The ASE of SOA_1 (green solid line) and ASE of SOA_2 (blue broken line) are shown in Figure 2. Even though all two SOAs are biased at the same current level of 200 mA, they exhibited different ASE spectra. The ASE data shown in Figure 3 shows that SOA_1 has higher gain than SOA_2 for the same bias current level, which implies that different bias current levels are required in order to get the same output power when the SOAs are individually used in the proposed fiber compound-ring resonator.

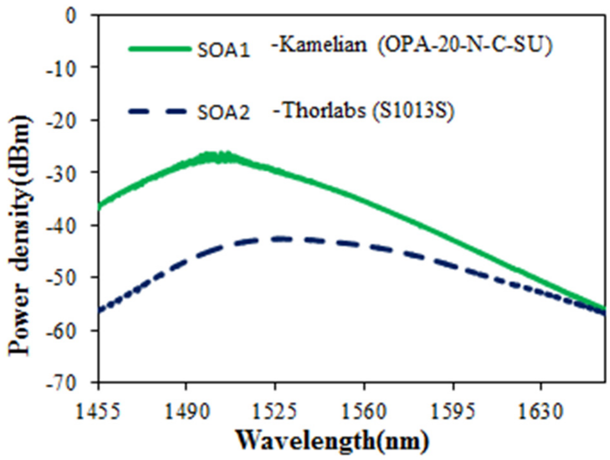

Figure 2. Amplified spontaneous emission (ASE) spectra of the SOA_1 (green solid line), and ASE of SOA_2 (blue broken line) of the fiber compound-ring laser with both two SOAs set at bias current I_B of 200 mA each.

4.2. Lasing Threshold Level

Each SOA was individually placed into the proposed fiber compound-ring cavity in order to determine the lasing threshold levels of the fiber compound-ring laser. The tunable filter was set at a 1550-nm wavelength. As shown in Figure 3a, the lasing starts when the bias current level is above 27 mA for the SOA_1 (Kamelian model) gain medium. On the other hand, the lasing starts when the bias current is above 180 mA for the SOA_2 (Thorlabs model) gain medium as shown in Figure 3b.

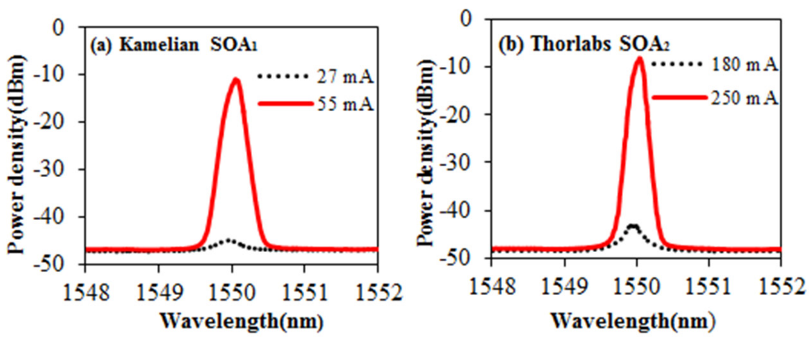

Figure 3. Illustrates the output spectra of the fiber laser threshold for each individual SOA gain medium. (**a**) shows the lasing threshold of the SOA_1; (**b**) shows the lasing threshold of the SOA_2 gain medium.

4.3. Tunable Optical Filter

The insertion losses (ILs) and corresponding full-width-half maximum (FWHM) linewidths within the entire tuning range (1520–1570 nm) of the tunable filter is shown in Figure 4. The insertion losses decrease as the wavelength increases. The maximum IL of 5.5 dB and minimum IL of 2.2 dB were measured at 1520 nm and 1570 nm, respectively. A similar downward trend was also noticed when the FWHM linewidths were plotted against the wavelengths as shown in Figure 4. The linewidth varies from 0.4 to 0.32 nm at 1520 and 1570 nm, respectively.

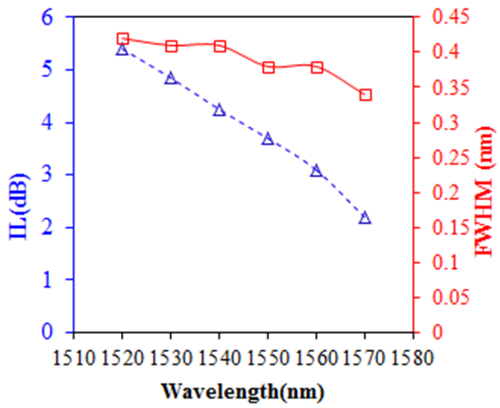

Figure 4. Insertion losses (IL, shown by triangles, in dB), and full-width-half maximum (FWHM, shown by squares, in nm) spectra of the tunable optical filter.

Due to the downward trend of the insertion losses from the tunable filter, an upward trend is also expected in the output power of the proposed fiber compound-ring laser for a constant gain setting of the SOAs. Consequently, a constant output power can be obtained over the entire wavelength tuning range by adjusting the bias current (I_B) of the SOAs but at the expense of signal broadening of the fiber laser source. The reflectivity of both SLMs was set at less than 0.1% so that both output ports of the fiber compound-ring lasers (i.e., OUT1 and OUT2) have the same output power. Then, by collecting both clockwise and counter-clockwise propagating light beams through the SLM_1 and SLM_2, respectively, we measured the 3-dB bandwidth at different bias current levels at the 1550-nm wavelength by using an OSA. The 3-dB bandwidth increased from 0.1985 to 0.2182 nm as the bias current was increased to the standard bias current of each of the SOAs (see Table 1).

Table 1. The 3-dB bandwidth (BW) at different bias current I_B (mA) levels and 1550-nm center wavelength with Sagnac loop mirror reflectivity set at <0.1%.

SOA_1 I_{B1} (mA)	SOA_2 I_{B2} (mA)	P_{OUT1} (dBm)	P_{OUT2} (dBm)	3 dB-BW (nm)
75	250	3.40	3.40	0.1985
100	300	5.80	5.70	0.2075
125	350	6.73	6.75	0.2122
150	400	7.65	7.68	0.2131
175	450	8.35	8.35	0.2157
200	500	8.94	8.95	0.2182

4.4. Coherent Beam Combining Efficiency

The principle of the proposed passive coherent beam combining technique of two compound-ring-based fiber lasers with two adjustable output couplers (i.e., Sagnac loop mirrors) is based on a passive phase-locking mechanism due to spontaneous self-organization operation [56,58]. Due to the wide bandwidth of the SOAs, the passive phase-locking mechanism allows the fields' self-adjustment to select common oscillating modes or resonant frequencies of the counter-propagating (i.e., clockwise and counter-clockwise) light beams in the two merged ring cavities and optimize their in-phase locking state conditions without any active phase modulating system.

In order to determine the beam combining efficiency of the proposed fiber laser structure, we first used each individual SOA as gain medium in the common branch I of the compound-ring cavity and measured the output power produced by the fiber laser system at its both output couplers, OUT1 and OUT2. Then, we placed at the same time both SOAs, SOA_1 (Kamelian model) and SOA_2 (Thorlabs, S1013S), in the compound-ring cavities (branch I and II, respectively). Similarly, we measured the output power delivered at both output couplers of the proposed fiber laser. Note that the reflectivity of the Sagnac loop mirrors, SLM_1 and SLM_2, was adjusted to maximum (i.e. >99.9%) and minimum (i.e., <0.1%), respectively. The tunable filter was manually adjusted from 1535 to 1565 nm and each semiconductor optical amplifier, SOA_1 and SOA_2, was driven and kept constant at its standard bias current, 200 and 500 mA, respectively. Figure 5 illustrates the passive coherent beam combining efficiency spectrum (right vertical axis) and the output power spectrum (left vertical axis) from the proposed fiber compound-ring laser operating with individual SOAs as well as both SOAs over the C-band tuning range of 30 nm.

The beam combining efficiency (filled circles) was obtained by dividing the optical power measured at the output port (OUT2) when the fiber laser was operating with both SOAs by the power summation (unfilled triangles) of the same output port of the fiber laser while operating with individual SOA, SOA_1 (filled squares) and SOA_2 (unfilled circles), i.e., $\eta = (P_{measured}/(P_{SOA1} + P_{SOA2}))$. The leakage optical power spectrum (unfilled squares) at the other output port (OUT_1) remained below −28.5 dBm. The maximum output power delivered by the fiber laser operating with a single SOA, SOA_1 (Kamelian model) and SOA_2 (Thorlabs model), was +8.91 and +8.90 dBm at 1565 nm, respectively. On the other hand, when both SOAs were placed in the compound-ring cavities, the maximum measured output power obtained at the output port, OUT2, was +11.9 dBm at 1565 nm, which is almost double the output power obtained with either individual SOA placed in the fiber compound-ring laser cavity. Moreover, the maximum output power obtained by just adding the optical power from single SOA fiber laser operation at the output port, OUT2, was +11.91 dBm vs. +11.9 dBm measured output power from the fiber laser operating with both SOAs at 1565 nm wavelength. This is where the insertion losses of the tunable filter were the lowest.

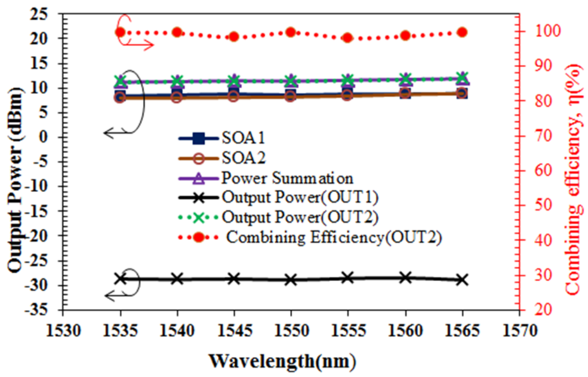

Figure 5. Output power and combining efficiency spectra of the proposed dual-Sagnac loop mirror SOA-based tunable fiber compound-ring laser system using two SOAs as gain media. Individual SOA output power spectrum: SOA_1 (filled squares), SOA_2 (unfilled circles), output power summation spectrum of both SOAs (unfilled triangles), and actual measured output power (crosses) at the output port, OUT2 with SOA_1 and SOA_2 driven at a 200-mA and 500-mA constant bias current. The PC_1 and PC_2 were maximized for each wavelength.

The maximum and minimum obtained combining efficiency (filled circles) was 99.76% and 98.06% at 1565 nm and 1555 nm, respectively, as shown in Figure 5 (right vertical axis).

4.5. Fiber Laser Power Tunability and its Switchable Dual-Output Port Operation

The proposed fiber compound-ring laser has a feature of operating with two adjustable and switchable output ports (i.e., OUT1 and OUT2). The output power from either output port can be tuned by adjusting the gain of the semiconductor amplifiers, SOA_1 and SOA_2, (i.e., by controlling their bias current levels) or by adjusting the reflectivity of the Sagnac loop mirrors, SLM_1 and SLM_2, while keeping the former constant.

The SOA gain adjustment method was performed by setting the tunable filter at 1550 nm wavelength and adjusting the bias current levels, I_{B1} and I_{B2} of both SOAs. Table 2 shows the output power evolution at both output ports, OUT1 and OUT2 as a function of the bias current levels, I_{B1} and I_{B2}. The reflectivity of the Sagnac loop mirror, SLM_1 and SLM_2 were set at $\geq$99.9% and $\leq$0.1%, respectively. The achieved maximum dynamic range was 40.75dB at both SOAs' standard bias current levels of 200 and 500 mA for SOA_1 and SOA_2, respectively.

Table 2. Optical power from the fiber laser output ports OUT1 and OUT2, at different bias current I_B (mA) levels and a 1550-nm center wavelength.

SOA_1 I_{B1} (mA)	SOA_2 I_{B2} (mA)	P_{OUT1} (dBm)	P_{OUT2} (dBm)
26	180	−36	−1.5
50	200	−32	5
75	250	−29.5	7.8
100	300	−28.9	9.3
150	400	−28.6	11.1
200	500	−28.9	11.85

The second approach involves the adjustment of the reflectivity of both Sagnac loop mirrors, SLM_1 and SLM_2 while keeping the gain of both SOAs constant (i.e., I_{B1} and I_{B2} set at 200 and 500 mA, respectively). The proposed fiber compound-ring laser can be operated in single or dual-output configuration depending on the reflectivity of the SLM1 and SLM_2.

In single output configuration, one of the Sagnac loop mirrors, SLM_1 or SLM_2, should be kept at high reflectivity (i.e., $\geq$99.9%) by adjusting its polarization controller, PC_4 or PC_5, respectively, while keeping the other Sagnac loop mirror at its lowest reflectivity of $\leq$0.1%.

The tunable filter was set at a 1550-nm wavelength in order to characterize the power tunability performance of both output ports of the fiber laser. Then, we initialized the reflectivity settings of the SLM_1 and SLM_2 to $\leq$0.1% and $\geq$99.9%, respectively. The initial measured output power from both output ports, OUT1 and OUT2, was +11.85 dBm and −28.9 dBm, respectively. Moreover, we gradually adjusted the reflectivity of the Sagnac loop mirror, SLM_1, by slowly changing the polarization state of the counter-propagating light beam into the SLM_1 by adjusting the polarization controller, PC_4, while recording the power meter readings at both output ports, OUT1 and OUT2. An optical spectrum analyzer (OSA) was used to record the reflectivity dependence of 3 dB-bandwidth of the output signal spectrum at the output port, OUT 1, We were able to control the output power from the output port, OUT1, from +11.85 dBm to −28.5 dBm while keeping the other output port, OUT2, at −28.9 dBm by also optimizing the polarization controller, PC_5, of SLM_2. Similarly, we also set the reflectivity of SLM_1 and SLM_2 to $\geq$99.9% and $\leq$0.1%, respectively, and checked both output ports' performance in the similar manner as stated above, where the measured output power from output port, OUT_2 was adjusted from +11.87 dBm to −28.9 dBm while keeping the output port, OUT1, at −28.9 dBm. Figure 6 illustrates the output power from both output ports, OUT1 (circles) and OUT2 (crosses) as a function of the reflectivity of the SLM_1. Note that both output ports behave similarly and the 3-dB bandwidth of the light beam from OUT1 (filled triangles increased as the reflectivity of the Sagnac loop mirror, SLM1, increased while the output power decreased as shown in Figure 6, due to the strong feedback (i.e., reflected light beam) from each SLMs.

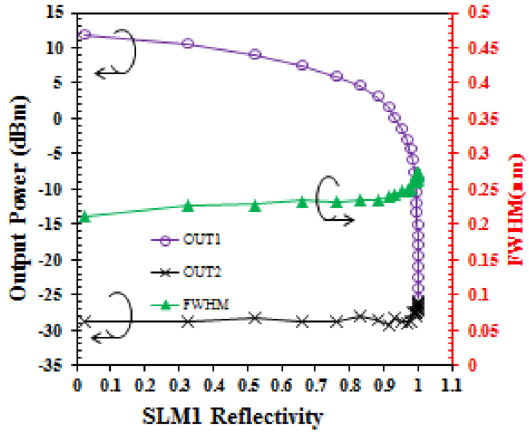

Figure 6. Shows the output power of output port, OUT1 (circles) and OUT2 (crosses), respectively, and the 3dB-bandwidth of output port, OUT1 (tringles) as a function of different reflectivity values of the Sagnac loop mirror, SML1, for single output port operation. FWHM: full-width-half maximum.

In a dual-output port configuration, both output ports can be fixed and also adjusted to any output power between +11.9 and −28.9 dBm. We firstly set both output ports, OUT1 and OUT2, to +8.94 and +8.95 dBm by adjusting the reflectivity of both Sagnac loop mirrors, SLM_1 and SLM_2 at ≤0.1%, as shown in Figure 7. Then, we gradually tuned the output power from the output port, OUT1, from +8.94 to −28.9 dBm by adjusting the reflectivity of the SLM_1 from 0.1% to more than 99.9% while optimizing the reflectivity of the SLM_2 in order to keep the output power at OUT2 constant at +8.95 dBm. The reflectivity of the SLM_2 was around 50% when the one of the SLM_1 was around 99.9% in order to maintain the output power at OUT2 constant at +8.95 dBm.

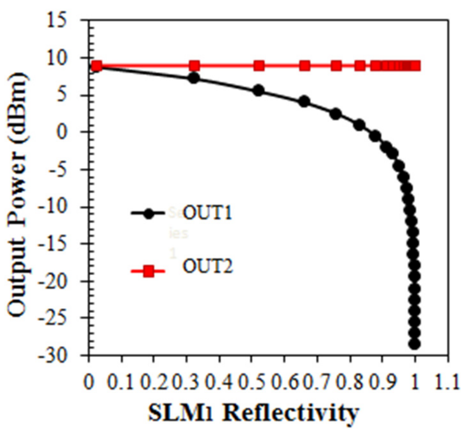

Figure 7. Illustrates the output power from both output ports, OUT1 (filled circles) and OUT2 (unfilled squares) for different reflectivity values of the Sagnac loop mirror, SLM_1 for dual-output port operation while keeping output power at OUT2 constant at +8.95 dBm.

4.6. Wavelength Tunability

The wavelength tuning range of the optical filter that was used in the proposed fiber laser was 50 nm (see Figure 4). Its maximum IL is 5.5 dB at 1520 nm and its minimum IL is 2.2 dB at 1570 nm. We first set the bias current for both SOAs at 200 and 500 mA, for SOA_1 and SOA_2, respectively. The reflectivity of the SLM_1 and SLM_2 were set and kept constant at ≤0.1% and ≥99.9%, respectively. Then, the wavelength of the output light beam was measured with an OSA, and was tuned by manually adjusting the tunable filter, from 1535 to 1565 nm while optimizing the polarization controllers, PC_1,

PC_2 and PC_3, at each wavelength of 1535, 1540, 1545, 1550, 1555, 1560 and 1565 nm as illustrated in Figure 8.

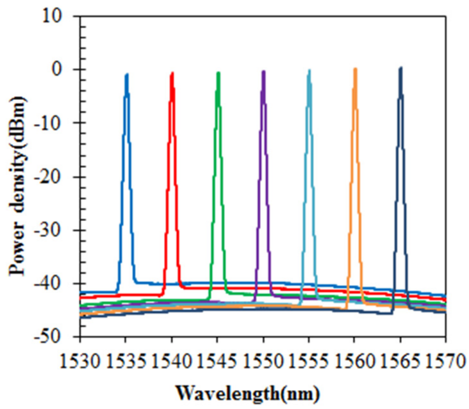

Figure 8. Shows the wavelength spectrum of the fiber compound-ring laser where PC_1, PC_2 and PC_3, were optimized at each wavelength.

4.7. Optical Signal-To-Noise Ratio

The measured peak signals from the optical spectrum analyzer for the above wavelength spectrum (see Figure 8) were used to determine the optical signal-to-noise ratio of the proposed fiber compound-ring laser by subtracting the peak power value at each center wavelength (i.e., 1535, 1540, 1545, 1550, 1555, 1560 and 1565 nm) from the background noise level of each wavelength spectrum (i.e., OSNR (dB) = $P_{Signal} - P_{Noise}$, where both P_{Signal} and P_{Noise} level are expressed in dBm), as demonstrated in Figure 9. The OSNR remained well above +39 dB over the whole wavelength tuning range, where the maximum OSNR of +44.6 dB was obtained at 1565 nm.

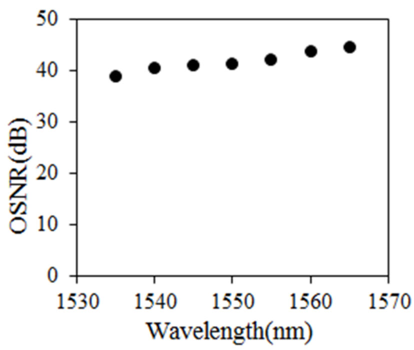

Figure 9. Shows the optical signal-to-noise ratio (OSNR) at each center wavelength spectrum, 1535, 1540, 1545, 1550, 1550, 1555, 1560 and 1565 nm with optimized PC_1, PC_2 and PC_3.

The obtained OSNR spectrum is in the range that is comparable to the OSNR levels for fiber lasers used in remote sensing [69,70], fiber sensors that utilize wavelength-peak measurement method [62] and optical communication systems [71].

4.8. Short-Term Optical Power

We finally performed the short-term optical power stability test at room temperature with SOA1, and SOA2 set at the standard bias current levels of 200 and 500 mA, respectively, while the tunable filter was set and kept fixed at a 1550-nm central wavelength. The OSA was also used to monitor and acquire the data. The optical stability test was carried out over a course of 180 min with time interval of 1 min, and OSA resolution bandwidth of 0.01 nm without additional data averaging.

Figure 10 shows the power stability measurements with fluctuations of less than ±0.02 dB, which indicates that the proposed fiber compound-ring laser is very stable. The power fluctuations during the stability measurement can be minimized by properly packaging the proposed fiber compound-ring laser system.

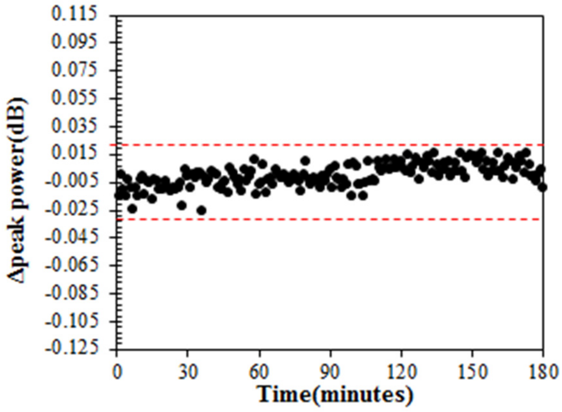

Figure 10. Shows the output power short-term fluctuations of the proposed fiber compound-ring laser at a 1550-nm wavelength.

5. (N >> 1) SOA-Based Fiber Compound-Ring Laser Structure

Passive coherent beam combining of two SOAs based fiber compound-ring laser has been demonstrated above with high beam combining efficiency without using any active phase modulators. The proposed fiber compound-ring cavity has great potential to achieve an efficient, stable, simple and inexpensive compact highly power-scalable fiber system by passively combining a [49,50] low power (N >> 1) number of SOAs fiber compound-ring lasers by using N × N fiber couplers with high beam combining efficiency. Estimation studies of beam combining efficiency have shown that it degrades as the number of individual combined Y-shaped linear cavity-based fiber lasers increases (i.e., N > 8) [72]. However, a large number of combined individual fiber lasers has been demonstrated in Y-shape coupled arrays [73] with high efficient coherent beam combining from 16 channels made by cascading two fiber laser arrays using EDFAs as gain medium. Thus, in addition to combining several arrays of compound-ring laser cavities, semiconductor optical amplifiers are the right candidates for the proposed (N >> 1) fiber laser compound-ring laser because they possess wide bandwidth to allow enough lasing modes within the actual gain bandwidth. Yet, we anticipate that the changes in the behavior of mode competition among the oscillating modes might lead to diminishing likelihood of obtaining the same spectral lasing mode [74,75]. Therefore, the beam combining efficiency is expected to degrade at very large number of combined arrays of merged compound-ring resonators. In addition, nonlinearities that manifest in semiconductor optical amplifier [76] as well as the optical damage and nonlinear effects, such as stimulated Raman scattering, stimulated Brillouin scattering and four-wave mixing in all-single-mode fiber output couplers, will become dominant at very high optical power and limit the maximum amount of optical power that can be achieved from the proposed fiber compound-ring laser.

Unlike previous work [51], the expensive high power combiner with a multimode fiber output port has been eliminated. The proposed SOA-based fiber compound-ring laser structure is a dual-output port all-single-mode-fiber laser structure that can be used in single or dual-output operation with adjustable output power. Figure 11. illustrates the proposed fiber laser structure with N × N fiber couplers and two Sagnac loop mirrors, SLM_1 and SLM_2, which form the output couplers, OUT1 and OUT1.

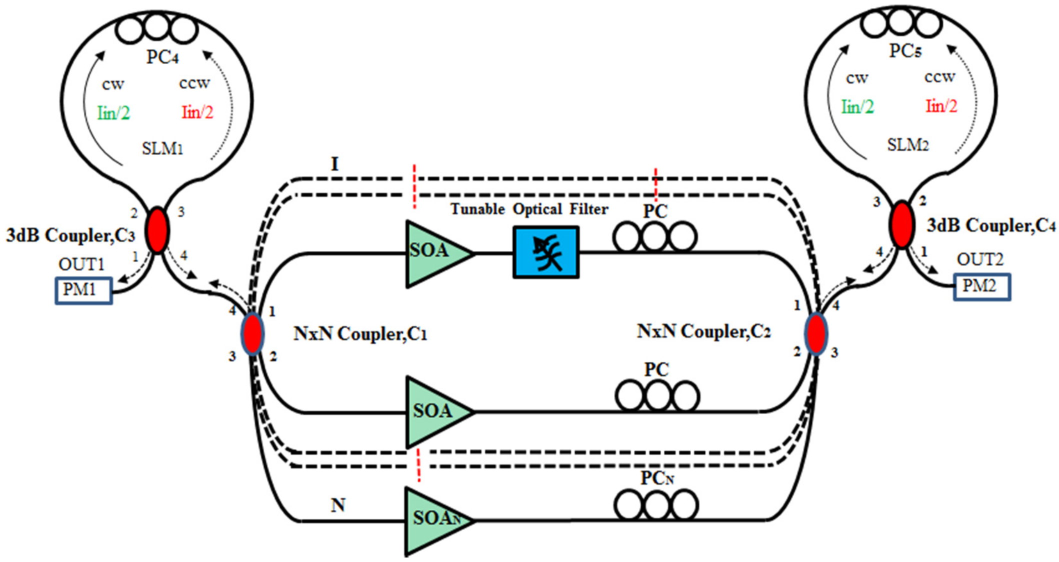

Figure 11. (N >> 1) number of SOA-based dual-output port fiber compound-ring laser structures.

6. Conclusions

Semiconductor optical amplifier-based fiber laser sources provide potential solutions for current optical technology because they are very compact, cost effective and user-friendly compared to their counterparts that utilize rare-earth ytterbium doped fiber amplifiers (YDFAs), erbium doped fiber amplifiers (EDFAs), stimulated Raman scattering (SRS) amplifiers or stimulated Brillouin scattering (SBS) amplifiers as well as free-space solid state laser sources.

In addition to using semiconductor optical amplifiers, the proposed compound-ring cavity does not contain any optical isolators or optical isolators, which can lead to the development of a simple and very high compact (i.e., on-chip scale) power scalable, adjustable and switchable laser source.

We successfully proposed and experimentally demonstrated very high coherent beam combining efficiency of two SOAs used as gain media in all-single-mode fiber compound-ring cavities with two switchable and power adjustable output couplers formed by using two Sagnac loop mirrors. The use of Sagnac loop mirrors eliminates the need of utilizing variable optical attenuators in order to adjust and control the laser output power. Two Sagnac loop mirrors have been used to switch the mode of operation of the proposed fiber laser from single output port to dual-output port operation as well as to adjust the output power on each output coupler. We have achieved more than 98% coherent beam combining efficiency of two parallel nested fiber ring resonators (i.e., compound-ring cavity) over the C-band tuning range of 30 nm. Optical signal-to -noise ratio (OSNR) of +45 dB, and optical power fluctuation of less than ± 0.02 dB were measured over the course of three hours at room temperature.

Finally, we discuss on how $N \times N$ fused fiber couplers can be used to achieve all-single-mode-fiber compound-ring laser structure with (N >> 1) number of SOAs that can be used for power scaling to achieve a high power laser source that simply uses low power optical components. Due to the advanced technologies of semiconductor optical amplifiers and tunable filters covering wide range of wavelength spectrum in different electromagnetic spectrum bands, the proposed fiber compound-ring laser can be used to build compact laser systems covering different optical wavelength-bands.

Acknowledgments: This research was support by Graduate Research Technology Initiative (GRTI) which is a CUNY internal grant.

Author Contributions: Muhammad A. Ummy conceived and designed the experiments; Simeon Bikorimana performed the experiments; Muhammad A. Ummy, Simeon Bikorimana and Roger Dorsinville analyzed the data; Muhammad A. Ummy and Roger Dorsinville contributed reagents/materials/analysis tools; Muhammad A. Ummy, Simeon Bikorimana and Roger Dorsinville wrote the paper.

Conflicts of Interest: The authors declare no conflict of interest.

References

1. He, X.; Fang, X.; Liao, C.; Wang, D.N.; Sun, J. A tunable and switchable single-longitudinal-mode dual-wavelength fiber laser with a simple linear cavity. *Opt. Express* **2009**, *17*, 21773–21781. [CrossRef] [PubMed]
2. Barnsley, P.; Urquhart, P.; Millar, C.; Brierley, M. Fiber Fox–Smith resonators: Application to single-longitudinal-mode operation of fiber lasers. *J. Opt. Soc. Am. A* **1988**, *5*, 1339–1346. [CrossRef]
3. Iwatsuki, K.; Takada, A.; Hagimoto, K.; Saruwatari, M.; Kimura, Y.; Shimizu, M. Er3+-doped Fiber-Ring-Laser with less than 10 kHz Linewidth. In Proceedings of the Optical Fiber Communication Conference, Houston, TX, USA, 6 February 1989.
4. Zhang, J.; Yue, C.Y.; Schinn, G.W.; Clements, W.R.L.; Lit, J.W.Y. Stable single-mode compound-ring erbium-doped fiber laser. *J. Lightwave Technol.* **1996**, *14*, 104–109. [CrossRef]
5. Chen, X.; Yao, J.; Deng, Z. Ultranarrow dual-transmission-band fiber Bragg grating filter and its application in a dual-wavelength single-longitudinal-mode fiber ring laser. *Opt. Lett.* **2005**, *30*, 2068–2070. [CrossRef] [PubMed]
6. Zhang, J.; Lit, J.W.Y. Compound fiber ring resonator: Theory. *J. Opt. Soc. Am. A* **1994**, *11*, 1867–1873. [CrossRef]
7. Urquhart, P. Compound optical-fiber-based resonators. *J. Opt. Soc. Am. A* **1988**, *5*, 803–812. [CrossRef]
8. Zhang, J.; Lit, J.W.Y. All-fiber compound ring resonator with a ring filter. *J. Lightwave Technol.* **1994**, *12*, 1256–1262.
9. Capmany, J.; Muriel, M.A. A new transfer matrix formalism for the analysis of fiber ring resonators: Compound coupled structures for FDMA demultiplexing. *J. Lightwave Technol.* **1990**, *8*, 1904–1919. [CrossRef]
10. Shi, W.; Fang, Q.; Zhu, X.; Norwood, R.A.; Peyghambarian, N. Fiber lasers and their applications [Invited]. *Appl. Opt.* **2014**, *53*, 6554–6568. [CrossRef] [PubMed]
11. Syms, R.R.A.; Zou, H.; Stagg, J.; Veladi, H. Sliding-blade MEMS iris and variable optical attenuator. *J. Micromech. Microeng.* **2004**, *14*, 1700. [CrossRef]
12. Unamuno, A.; Uttamchandani, D. MEMS variable optical attenuator with Vernier latching mechanism. *IEEE Photonics Technol. Lett.* **2006**, *18*, 88–90. [CrossRef]
13. Marxer, C.; Griss, P.; de Rooij, N.F. A variable optical attenuator based on silicon micromechanics. *IEEE Photonics Technol. Lett.* **1999**, *11*, 233–235. [CrossRef]
14. Li, Q.; Au, A.A.; Lin, C.-H.; Lyons, E.R.; Lee, H.P. An efficient all-fiber variable optical attenuator via acoustooptic mode coupling. *IEEE Photonics Technol. Lett.* **2002**, *14*, 1563–1565.
15. Duduś, A.; Blue, R.; Zagnoni, M.; Stewart, G.; Uttamchandani, D. Modeling and Characterization of an Electrowetting-Based Single-Mode Fiber Variable Optical Attenuator. *IEEE J. Sel. Top. Quantum Electron.* **2015**, *21*, 253–261. [CrossRef]
16. Benner, A.; Presby, H.M.; Amitay, N. Low-reflectivity in-line variable attenuator utilizing optical fiber tapers. *J. Lightwave Technol.* **1990**, *8*, 7–10. [CrossRef]
17. Kerbage, C.; Hale, A.; Yablon, A.; Windeler, R.S.; Eggleton, B.J. Integrated all-fiber variable attenuator based on hybrid microstructure fiber. *Appl. Phys. Lett.* **2001**, *79*, 3191–3193. [CrossRef]
18. Lim, K.S.; Pua, C.H.; Harun, S.W.; Ahmad, H. Temperature-sensitive dual-segment polarization maintaining fiber Sagnac loop mirror. *Opt. Laser Technol.* **2010**, *42*, 377–381. [CrossRef]
19. Sun, G.; Moon, D.S.; Chung, Y. Simultaneous Temperature and Strain Measurement Using Two Types of High-Birefringence Fibers in Sagnac Loop Mirror. *IEEE Photonics Technol. Lett.* **2007**, *19*, 2027–2029. [CrossRef]
20. Fu, H.Y.; Tam, H.Y.; Shao, L.-Y.; Dong, X.; Wai, P.K.A.; Lu, C.; Khijwania, S.K. Pressure sensor realized with polarization-maintaining photonic crystal fiber-based Sagnac interferometer. *Appl. Opt.* **2008**, *47*, 2835–2839. [CrossRef] [PubMed]
21. Das, G.; Lit, J.W.Y. Wavelength switching of a fiber laser with a Sagnac loop reflector. *IEEE Photonics Technol. Lett.* **2004**, *16*, 60–62. [CrossRef]
22. Lim, D.S.; Lee, H.K.; Kim, K.H.; Kang, S.B.; Ahn, J.T.; Jeon, M.Y. Generation of multiorder Stokes and anti-Stokes lines in a Brillouin erbium-fiber laser with a Sagnac loop mirror. *Opt. Lett.* **1998**, *23*, 1671–1673. [CrossRef] [PubMed]

23. Wang, S.S.; Hu, Z.F.; Li, Y.H.; Tong, L.M. All-fiber Fabry–Perot resonators based on microfiber Sagnac loop mirrors. *Opt. Lett.* **2009**, *34*, 253–255. [CrossRef] [PubMed]
24. Ummy, M.A.; Madamopoulos, N.; Lama, P.; Dorsinville, R. Dual Sagnac loop mirror SOA-based widely tunable dual-output port fiber laser. *Opt. Express* **2009**, *17*, 14495–14501. [CrossRef] [PubMed]
25. Ummy, M.A.; Madamopoulos, N.; Joyo, A.; Kouar, M.; Dorsinville, R. Tunable multi-wavelength SOA based linear cavity dual-output port fiber laser using Lyot-Sagnac loop mirror. *Opt. Express* **2011**, *19*, 3202–3211. [CrossRef] [PubMed]
26. Mortimore, D.B. Fiber loop reflectors. *J. Lightwave Technol.* **1988**, *6*, 1217–1224. [CrossRef]
27. Feng, S.; Mao, Q.; Shang, L.; Lit, J.W. Reflectivity characteristics of the fiber loop mirror with a polarization controller. *Opt. Commun.* **2007**, *277*, 322–328. [CrossRef]
28. Klingebiel, S.; Röser, F.; Ortaç, B.; Limpert, J.; Tünnermann, A. Spectral beam combining of Yb-doped fiber lasers with high efficiency. *J. Opt. Soc. Am. B* **2007**, *24*, 1716–1720. [CrossRef]
29. Raab, V.; Menzel, R. External resonator design for high-power laser diodes that yields 400 mW of TEM_{00} power. *Opt. Lett.* **2002**, *27*, 167–169. [CrossRef] [PubMed]
30. Corcoran, C.J.; Rediker, R.H. Operation of five individual diode lasers as a coherent ensemble by fiber coupling into an external cavity. *Appl. Phys. Lett.* **1991**, *59*, 759–761. [CrossRef]
31. Liu, B.; Braiman, Y. Coherent beam combining of high power broad-area laser diode array with near diffraction limited beam quality and high power conversion efficiency. *Opt. Express* **2013**, *21*, 31218–31228. [CrossRef] [PubMed]
32. Daneu, V.; Sanchez, A.; Fan, T.Y.; Choi, H.K.; Turner, G.W.; Cook, C.C. Spectral beam combining of a broad-stripe diode laser array in an external cavity. *Opt. Lett.* **2000**, *25*, 405–407. [CrossRef] [PubMed]
33. Loftus, T.H.; Liu, A.; Hoffman, P.R.; Thomas, A.M.; Norsen, M.; Royse, R.; Honea, E. 522 W average power, spectrally beam-combined fiber laser with near-diffraction-limited beam quality. *Opt. Lett.* **2007**, *32*, 349–351. [CrossRef] [PubMed]
34. Fan, T.Y. Laser beam combining for high-power, high-radiance sources. *IEEE J. Sel. Top. Quantum Electron.* **2005**, *11*, 567–577. [CrossRef]
35. Augst, S.J.; Goyal, A.K.; Aggarwal, R.L.; Fan, T.Y.; Sanchez, A. Wavelength beam combining of ytterbium fiber lasers. *Opt. Lett.* **2003**, *28*, 331–333. [CrossRef] [PubMed]
36. Wirth, C.; Schmidt, O.; Tsybin, I.; Schreiber, T.; Peschel, T.; Brückner, F.; Clausnitzer, T.; Limpert, J.; Eberhardt, R.; Tünnermann, A.; et al. 2 kW incoherent beam combining of four narrow-linewidth photonic crystal fiber amplifiers. *Opt. Express* **2009**, *17*, 1178–1183. [CrossRef] [PubMed]
37. Sprangle, P.; Ting, A.; Penano, J.; Fischer, R.; Hafizi, B. Incoherent Combining and Atmospheric Propagation of High-Power Fiber Lasers for Directed-Energy Applications. *IEEE J. Quantum Electron.* **2009**, *45*, 138–148. [CrossRef]
38. Sabourdy, D.; Kermène, V.; Desfarges-Berthelemot, A.; Vampouille, M.; Barthélémy, A. Coherent combining of two Nd: YAG lasers in a Vernier–Michelson-type cavity. *Appl. Phys. B* **2002**, *75*, 503–507. [CrossRef]
39. Bloom, G.; Larat, C.; Lallier, E.; Carras, M.; Marcadet, X. Coherent combining of two quantum-cascade lasers in a Michelson cavity. *Opt. Lett.* **2010**, *35*, 1917–1919. [CrossRef] [PubMed]
40. Sabourdy, D.; Kermène, V.; Desfarges-Berthelemot, A.; Lefort, L.; Barthélémy, A.; Even, P.; Pureur, D. Efficient coherent combining of widely tunable fiber lasers. *Opt. Express* **2003**, *11*, 87–97. [CrossRef] [PubMed]
41. Jeux, F.; Desfarges-Berthelemot, A.; Kermène, V.; Barthelemy, A. Experimental demonstration of passive coherent combining of fiber lasers by phase contrast filtering. *Opt. Express* **2012**, *20*, 28941–28946. [CrossRef] [PubMed]
42. Kozlov, V.A.; Hernández-Cordero, J.; Morse, T.F. All-fiber coherent beam combining of fiber lasers. *Opt. Lett.* **1999**, *24*, 1814–1816. [CrossRef] [PubMed]
43. Moon, D.S.; Kim, B.H.; Lin, A.; Sun, G.; Han, W.T.; Han, Y.G.; Chung, Y. Tunable multi-wavelength SOA fiber laser based on a Sagnac loop mirror using an elliptical core side-hole fiber. *Opt. Express* **2007**, *15*, 8371–8376. [CrossRef] [PubMed]
44. Kim, C.S.; Sova, R.M.; Kang, J.U. Tunable multi-wavelength all-fiber Raman source using fiber Sagnac loop filter. *Opt. Commun.* **2003**, *218*, 291–295. [CrossRef]
45. Zverev, P.G.; Basiev, T.T.; Prokhorov, A.M. Stimulated Raman scattering of laser radiation in Raman crystals. *Opt. Mater.* **1999**, *11*, 335–352. [CrossRef]

46. Smith, S.P.; Zarinetchi, F.; Ezekiel, S. Narrow-linewidth stimulated Brillouin fiber laser and applications. *Opt. Lett.* **1991**, *16*, 393–395. [CrossRef] [PubMed]
47. Yong, J.C.; Thévenaz, L.; Kim, B.Y. Brillouin Fiber Laser Pumped by a DFB Laser Diode. *J. Lightwave Technol.* **2003**, *21*, 546. [CrossRef]
48. Lowery, A.J.; Premaratne, M. Design and simulation of a simple laser rangefinder using a semiconductor optical amplifier-detector. *Opt. Express* **2005**, *13*, 3647–3652. [CrossRef] [PubMed]
49. Lowery, A.J.; Premaratne, M. Reduced component count optical delay discriminator using a semiconductor optical amplifier-detector. *Opt. Express* **2005**, *13*, 290–295. [CrossRef] [PubMed]
50. Premaratne, M.; Lowery, A.J. Analytical characterization of SOA-based optical pulse delay discriminator. *J. Lightwave Technol.* **2005**, *23*, 2778–2787. [CrossRef]
51. Arez, N.; Razaghi, M. Optical and logic gate implementation using four wave mixing in semiconductor optical amplifier for high speed optical communication systems. In Proceedings of the International Conference on Network and Electronics Engineering, Singapore, 16–18 September 2011; pp. 65–70.
52. Das, N.; Razaghi, M.; Hosseini, R. Four-wave mixing in semiconductor optical amplifiers for high-speed communications. In Proceedings of the 5th International Conference on Computers and Devices for Communication (CODEC), Kolkata, India, 17–19 December 2012.
53. Das, N.K.; Yamayoshi, Y.; Kawaguchi, H. Analysis of basic four-wave mixing characteristics in a semiconductor optical amplifier by the finite-difference beam propagation method. *IEEE J. Quantum Electron.* **2000**, *36*, 1184–1192.
54. Sato, K.; Toba, H. Reduction of mode partition noise by using semiconductor optical amplifiers. *IEEE J. Sel. Top. Quantum Electron.* **2001**, *7*, 328–333. [CrossRef]
55. Takano, K.; Nakagawa, K.; Takahashi, Y.; Ito, H. Reduction of Power Fluctuation in Pulsed Lightwave Frequency Sweepers with SOA Following EDFA. *IEEE Photonics Technol. Lett.* **2007**, *19*, 525–527. [CrossRef]
56. Bruesselbach, H.; Jones, D.C.; Mangir, M.S.; Minden, M.; Rogers, J.L. Self-organized coherence in fiber laser arrays. *Opt. Lett.* **2005**, *30*, 1339–1341. [CrossRef] [PubMed]
57. Lhermite, J.; Desfarges-Berthelemot, A.; Kermene, V.; Barthelemy, A. Passive phase locking of an array of four fiber amplifiers by an all-optical feedback loop. *Opt. Lett.* **2007**, *32*, 1842–1844. [CrossRef] [PubMed]
58. Lei, B.; Feng, Y. Phase locking of an array of three fiber lasers by an all-fiber coupling loop. *Opt. Express* **2007**, *15*, 17114–17119. [CrossRef] [PubMed]
59. Ummy, M.A.; Bikorimana, S.; Madamopoulos, N.; Dorsinville, R. Beam Combining of SOA-Based Bidirectional Tunable Fiber Nested Ring Lasers With Continuous Tunability Over the C-band at Room Temperature. *J. Lightwave Technol.* **2016**, *34*, 3703–3710. [CrossRef]
60. Cariou, J.P.; Augere, B.; Valla, M. Laser source requirements for coherent lidars based on fiber technology. *C. R. Phys.* **2006**, *7*, 213–223. [CrossRef]
61. Martinez-Ríos, A.; Anzueto-Sanchez, G.; Selvas-Aguilar, R.; Guzman, A.A.C.; Toral-Acosta, D.; Guzman-Ramos, V.; Duran-Ramirez, V.M.; Guerrero-Viramontes, J.A.; Calles-Arriaga, C.A. High sensitivity fiber laser temperature sensor. *IEEE Sens. J.* **2015**, *5*, 2399–2402. [CrossRef]
62. Pham, T.B.; Bui, H.; Le, H.T.; Pham, V.H. Characteristics of the Fiber Laser Sensor System Based on Etched-Bragg Grating Sensing Probe for Determination of the Low Nitrate Concentration in Water. *Sensors* **2016**, *17*, 7. [CrossRef] [PubMed]
63. Fu, H.; Chen, D.; Cai, Z. Fiber sensor systems based on fiber laser and microwave photonic technologies. *Sensors* **2012**, *12*, 5395–5419. [CrossRef] [PubMed]
64. Park, N.S.; Chun, S.K.; Han, G.H.; Kim, C.S. Acousto-Optic–Based Wavelength-Comb-Swept Laser for Extended Displacement Measurements. *Sensors* **2017**, *17*, 740. [CrossRef] [PubMed]
65. Peng, P.C.; Lin, J.H.; Tseng, H.Y.; Chi, S. Intensity and wavelength-division multiplexing FBG sensor system using a tunable multiport fiber ring laser. *IEEE Photonics Technol. Lett.* **2004**, *16*, 230–232. [CrossRef]
66. Delorme, F. Widely tunable 1.55 μm lasers for wavelength-division-multiplexed optical fiber communications. *IEEE J. Sel. Top. Quantum Electron.* **1998**, *34*, 1706–1716. [CrossRef]
67. Yun, S.H.; Tearney, G.J.; de Boer, J.F.; Iftimia, N.; Bouma, B.E. High-speed optical frequency-domain imaging. *Opt. Express* **2003**, *11*, 2953–2963. [CrossRef] [PubMed]
68. Hemmer, E.; Benayas, A.; Légaré, F.; Vetrone, F. Exploiting the biological windows: Current perspectives on fluorescent bioprobes emitting above 1000 nm. *Nanoscale Horiz.* **2016**, *1*, 168–184. [CrossRef]

69. Wang, G.; Zhan, L.; Liu, J.; Zhang, T.; Li, J.; Zhang, L.; Peng, J.; Yi, L. Watt-level ultrahigh-optical signal-to-noise ratio single-longitudinal-mode tunable Brillouin fiber laser. *Opt. Lett.* **2013**, *38*, 19–21. [CrossRef] [PubMed]
70. Luo, Y.; Tang, Y.; Yang, J.; Wang, Y.; Wang, S.; Tao, K.; Zhan, L.; Xu, J. High signal-to-noise ratio, single-frequency 2 μm Brillouin fiber laser. *Opt. Lett.* **2014**, *39*, 2626–2628. [CrossRef] [PubMed]
71. Yan, L.S.; Yao, X.S.; Shi, Y.; Willner, A.E. Simultaneous monitoring of both optical signal-to-noise ratio and polarization-mode dispersion using polarization scrambling and polarization beam splitting. *J. Lightwave Technol.* **2005**, *23*, 3290. [CrossRef]
72. Kouznetsov, D.; Bisson, J.; Shirakawa, A.; Ueda, K. Limits of coherent addition of lasers: Simple estimate. *Opt. Rev.* **2005**, *12*, 445–447. [CrossRef]
73. Chang, W.; Wu, T.; Winful, H.; Galvanauskas, A. Array size scalability of passively coherently phased fiber laser arrays. *Opt. Express* **2010**, *18*, 9634–9642. [CrossRef] [PubMed]
74. Sivaramakrishnan, S.; Chang, W.; Galvanauskas, A.; Winful, H.G. Dynamics of Passively Phased Ring Oscillator Fiber Laser Arrays. *IEEE J. Quantum Electron.* **2015**, *51*, 1–9. [CrossRef]
75. Bochove, E.J.; Shakir, S.A. Analysis of a spatial-filtering passive fiber laser beam combining system. *IEEE J. Sel. Top. Quantum Electron.* **2009**, *15*, 320–327. [CrossRef]
76. Barua, S.; Das, N.; Nordholm, S.; Razaghi, M. Comparison of pulse propagation and gain saturation characteristics among different input pulse shapes in semiconductor optical amplifiers. *Opt. Commun.* **2016**, *359*, 73–78. [CrossRef]